Journal of Manufacturing Processes 60 (2020) 673–683

Contents lists available at ScienceDirect

Journal of Manufacturing Processes

journal homepage: www.elsevier.com/locate/manpro

Induction melt thermoforming of advanced multi-axial thermoplastic composite laminates

P. Harrison [a], I. Campbell [a,*], E. Guliyev [a], B. McLelland [a], R. Gomes [b], N. Curado-Correia [b], E. McGookin [a], D.M. Mulvihill [a]

[a] James Watt School of Engineering, University of Glasgow, University Avenue, G12 8QQ, United Kingdom
[b] INEGI, Composite Materials and Structures Research, Institute of Mechanical Engineering and Industrial Management, Porto 4200-465, Portugal

ARTICLE INFO

Keywords:
Forming
Thermoplastic resin
Carbon fibres
Defects

ABSTRACT

The viability of using induction heating to facilitate the wrinkle-free forming of multi-axial pre-consolidated advanced thermoplastic composites over complex geometries is explored. The research focuses on the use of tin as a medium to both heat and lubricate the forming laminate. Initial tests demonstrate the viability of the fundamental ideas of the process; induction heating is used to melt the tin sheet, which is then shown to melt the matrix phase of carbon-nylon composite laminates when stacked in a hybrid composite/tin layup. A novel low-cost reconfigurable multi-step forming tool is used to demonstrate how most of the tin can be squeezed out of the layup prior to consolidation. The multi-step tool can be augmented with segmented tooling to rapidly manufacture composite parts of high geometric complexity. In this investigation, a 'ripple' geometry containing three 'cavities' is used to demonstrate the technique. Tests demonstrated that at least three sheets of inter-laminar tin can be simultaneously melted using the induction heating system. Initial results indicate complex geometries can be formed with minimal wrinkling while removing interlaminar tin.

1. Introduction

If the inherent difficulties in manufacturing with advanced thermoplastic composites can be overcome, they offer a route to rapid production of high performance (light-weight, tough, corrosion resistant, recyclable) structural components. Rapid thermo-forming of advanced thermoplastic composite laminates [1–15] is of particular interest in the automotive industry due to the changing economics caused by legislative pressure to reduce emissions and improve recyclability [16]. This pressure is increasing the viability of advanced thermoplastic composites in replacing more traditional heavier materials. However, without significant reductions in their material and manufacturing cost, their exploitation will be restricted to niche, high-end markets. Only by understanding and solving the fundamental problems involved in processing these materials can their potential be fully exploited in the much larger, lower cost markets. Despite the development of sheet forming processes for advanced composites dating back over 30 years [17], including matched-die press forming [2,4–7,12,13,18,19], vacuum forming [20,21], rubber forming [1], hydro forming [10,11,22] and diaphragm forming [8,23], various processing issues have yet to be satisfactorily resolved. This investigation focuses on two important such problems and explores solutions to both.

- *Problem 1: How to press-form complex components from pre-consolidated multi-axial thermoplastic laminates without inducing wrinkles?*
- *Problem 2: How to press-form highly complex geometries with multiple cavities, without inducing defects due to bridging and tearing of the forming laminate?*

Typically, to achieve optimum mechanical properties of structural components, placement of fibres is required in multiple directions to accommodate complex loading conditions. While wrinkle-free forming of biaxial thermoset or thermoplastic pre-impregnated sheets is relatively simple e.g. [2,4–6,12,14,18,23,24], forming pre-consolidated multi-axial sheets without wrinkles is more challenging, but of potentially greater utility due to the increased design flexibility afforded by multi-axial sheets [1,8–12,21,22,25–27]. The problem of forming multi-axial pre-consolidated laminates is that the ply configuration can induce large relative displacements between adjacent, but differently orientated, pairs of plies within the blank when formed over doubly curved geometries. Large inter-ply shear stresses at the interfaces between initially non-orthogonal plies result. For example, in a

* Corresponding author.
E-mail address: i.campbell.3@research.gla.ac.uk (I. Campbell).

https://doi.org/10.1016/j.jmapro.2020.10.026
Received 22 June 2020; Received in revised form 18 September 2020; Accepted 7 October 2020
Available online 17 November 2020

[0°/90°|45°/-45°|90°/0°] layup, the interfaces indicated by "|" tend to generate significant inter-ply shear and compressive stresses ultimately resulting in out-of-plane wrinkling [9,26] (a comprehensive review of other reasons for wrinkle generation when forming multi-layer laminates of engineering fabric is provided by Thompson et al. [28]). Unwanted wrinkles frozen into the final manufactured structural part can lead to significant knock-downs in strength of up to 70 % [29,30]. Consequently, mitigating wrinkles during forming is an important challenge and various approaches have been explored. It has been shown that decreasing the forming rate, increasing diaphragm stiffness and decreasing pre-form thickness all reduce wrinkling during isothermal diaphragm forming [8]. A method of reducing the mechanical coupling, and therefore the shear stress, at interfaces involving large relative displacements during press-forming was proposed and tested by Vanclooster [31]. Thin sheets of neat thermoplastic polymer matrix were added, effectively lubricating the tangential slip between these layers. The technique significantly improved formability by reducing wrinkling, but also resulted in a lower fibre volume fraction in the formed part, decreasing final specific mechanical properties. Two more recent investigations [21,26] explored the effect of stacking sequence in multi-axial carbon/epoxy prepreg blanks on wrinkling and concluded that 'using a good stacking sequence appears to be the only reliable method of overcoming any tendency of wrinkle development' [26]. Attempts to reduce wrinkling met with limited success despite using a mould tool of relatively simple geometric complexity. Various studies have looked into the use of segmented blank-holders in controlling deformation and wrinkles [18,32]. Improved results have been obtained for dry fabric multi-layer preforms using rigid interlayers constrained within a piezo-actuated blank-holder system [33], however the method is less applicable for use with 'viscous' pre-impregnated laminates.

At present, the problem of wrinkling in pre-consolidated multi-axial laminates remains severe, especially when considering tooling of high geometric complexity. In addition to wrinkling of multi-axial advanced composite prepreg blanks, problems also occur when forming complex geometries containing multiple cavities; namely 'bridging' and 'tearing'. Multiple cavities in a given geometry can lead to trapping of the forming sheet, leading to considerable tensile stress. This effect is exploited in stretch-forming of metals where a draw-bead is used to control tension and tensile strains. Unlike stretch-formed metal alloys that can deform plastically in all directions, advanced composites are almost inextensible in the fibre directions. Consequently, if the applied forming pressure is relatively low, for example in diaphragm forming, fibres resist drawing into cavities and bridge across them instead [20]. If the applied forming pressure is relatively high, as in press forming, fibres can tear due to excessive tensile loads generated by high frictional forces [13]. To avoid bridging and tearing, complex multi-cavity geometries like the 'curve--glide' geometry formed by [34] are generally manufactured by hand in a sequential forming operation. Attempts to stamp form such a complex multi-cavity shape in one vertical forming step using two rigid tools could result in tearing of the blank, due to the large draw-in displacements and high friction generated shear stresses between the composite blank and the tool.

A novel solution to forming wrinkle-free multi-axial pre-consolidated laminates into multi-cavity geometries is considered in this investigation. Combining incremental matched-die press forming [19] and diaphragm forming methods [17], the technique also involves a variation of the method devised by Vanclooster [31]. Here, instead of using molten thermoplastic polymer inter-layers to reduce the mechanical coupling [35], the idea is to use molten metal interlayers, heated rapidly and efficiently via induction heating. This 'inside-out' mode of heating also brings advantages to high-temperature diaphragm forming. In contrast to radiant [2] or convection heating [8], the rubber sheet is the last material to be exposed to high temperatures. It is therefore, less likely to fail and this method allows for cycle times measured in seconds rather than minutes [8].

The very low viscosity (about 1/10,000th that of a molten thermoplastic polymer) dramatically reduces the coupling between differently orientated pairs of composite plies, effectively lubricating the interface and reducing the shear stresses. An automatic multi-step forming process, involving a novel segmented male punch design, is used to create a squeeze-flow [36] with the pressure gradient directed from the centre towards the outer perimeter of the molten laminate. The low viscosity molten metal is squeezed out of the laminate during the forming process and the high surface tension of the molten metal and subsequent low wettability between the molten metal and the molten composite means that almost all of the molten metal can exit the laminate - ideally leaving very little metal within the formed part. The metal may subsequently be collected within the silicone rubber diaphragms and reused after each forming operation, thereby reducing costs. The multi-step forming process also provides a solution to automated forming of multi-cavity geometries, mitigating bridging and tearing of the laminate. For the method to work, the relative melt temperatures of the composite and metal must be well-chosen: an ideal system to investigate the concept is carbon-nylon thermoplastic composite & pure tin. The melt temperature of nylon is ~220−235 °C, while that of pure tin is 232 °C. The latter has a viscosity of about ~2 mPas at 250 °C [37] and a surface tension of ~600 mN m^{-1} at 235 °C [38], about two and eight times that of water respectively. The hybrid laminates are thermoformed at over 240 °C, where both composite and tin co-exist in a molten state.

The remainder of this paper is structured as follows: Section 2 summarises the steps involved in realising a functioning process. Section 3 presents the results of forming attempts with both flat and ripple tooling geometries and with both single and multilayer tin layups and Section 4 concludes the work. It is important to emphasise that the focus of this paper is on establishing the novel process itself and giving an initial assessment of its general effectiveness and viability. In this case, there were many complex technological challenges involved in achieving a working process while operating under a time limit enforced by equipment rental – especially in simultaneously incorporating induction heating, molten metal processing and multi-step forming in a composite forming process. Therefore, detailed mechanical, optical and radiographic characterisation of the formed parts is left to a follow-on paper.

2. Materials and experimental setup

2.1. Materials

Pre-consolidated sheets were made from carbon fibre – nylon composite consisting of four plies of TenCate Cetex® TC910 Nylon 6 UD tape [40] in a [0°/90°/90°/0°] layup, initially bonded together using ultrasonic spot welding before being fully consolidated using a pressure of 5.9 bar at 270 °C. The thickness of the tape is 0.16 mm. The fibre volume fraction is 49 % and the polymer content is 40 % by weight. The average thickness of the laminate is 0.68 mm with a standard deviation of 0.10 mm. The recommended processing temperature is 249 °C–271 °C. The matrix polymer is Ultramid B3W (PA6) which has a melt temperature of 223.4 °C. The forming behaviour of the laminates was recently reported in [39]. Limited rate and temperature dependent viscosity data for the matrix polymer are provided in the supplier's datasheet (TenCate). Laminates of various layups were created from the [0°/90°/90°/0°] pre-consolidated carbon fibre – nylon composite and tin sheets. Silex Silicones high temperature silicone sheet was used as the upper and lower diaphragm material. The maximum operating temperature of the silicone rubber is between 300−315 °C, its thickness is 0.3 mm. Tin shot purchased from Alfa Aesar was used to manufacture tin sheet measuring 1 × 150 × 150 (mm) using a bespoke aluminium mould. The mould allowed recycling of the tin after each forming experiment, significantly reducing costs.

2.2. Experimental setup

2.2.1. Overview

A schematic of the basic set up is shown in Fig. 1a and 1b. Fig. 1b (i) shows the segmented male tooling. In (ii) there is a cross section view of the Carbon-Nylon-Tin sample within the Silicone Diaphragm. In (iii) the vacuum pump is connected creating 1 bar of consolidation pressure. At (iv) a blank holder secures a double-diaphragm arrangement consisting of silicone rubber sheets into which the composite and metal interlayers are placed. (v) shows a false base plate located in the bed of the universal test machine upon which (vi) the segmented female tooling mounted on. (vii) An induction coil is placed just below the false base plate allowing *in-situ* heating. The distance, d1, is the gap between the coil and the sample. d1 was 25 mm when forming flat geometries and 60 mm when forming ripple geometries. The increase in d1 was necessary to safely position the Female Tooling.

2.2.2. Lower thermoforming setup

Fig. 2a shows the lower setup depicted in Fig. 1b (iv-vii), prior to placing the diaphragm and blank in the test machine (a Zwick Z250 Universal with 250 kN load cell). Two identical Perspex rings, a lower ring and an upper ring are separated by six wooden dowels, secured using orange 3-D printed ABS plastic supports bonded to the lower and upper rings. Inside the Perspex rings is positioned a non-electrically conductive glass/epoxy 'false base plate', manufactured via vacuum infusion and supported by four wooden legs with white ABS printed supports. Directly below the false base plate is a water cooled copper helical induction coil manufactured by Induction Coil Solutions and powered by a 12 kW, 80 kHz induction heating unit from Ceia, controlled by a V6 Control unit. This setup allows *in-situ* heating and pressing of the composite/tin specimens with no need for a shuttle system. The surface temperature of the upper diaphragm was monitored using both a FLIR One Pro thermal imaging camera and an Etekcity Lasergrip 1080 non-contact digital laser infrared thermometer (both use a wavelength range of 8−14 μm). When forming complex geometries, the female tool (see Section 2.2.3) is placed on top of the false base-plate, underneath the silicone diaphragm. The motivations for using a silicone diaphragm were five-fold: ***(i) safety*** – without proper care, molten tin can be dangerous. A silicone diaphragm constrains the liquid tin during the press-forming process, minimising the risk of burns and facilitating collection of the tin after forming ***(ii) fixed position and tensioning*** – the diaphragm holds the specimen in place resisting the force generated by the induction coil and it also imparts tensile stresses during forming, reducing the sheet's tendency to wrinkle, ***(iii) consolidation*** – application of a vacuum automatically provides 1 bar of consolidation pressure and ***(iv) oxidisation*** – the absence of air mitigates oxidisation of the molten tin improving the potential for recycling via recasting into tin sheet ***(v) air ingress*** – when molten, the surface tension of the tin tends to increase the thickness of the tin sheet, inducing a dendritic pattern formation which, without the diaphragm, would draw air into the laminate, disrupting circulating eddy currents and generating heterogeneous temperature distributions across the sheet. Drawing a vacuum inside the silicone diaphragm prevents air ingress. Both the base-plate and the female tool must be electrical insulators to allow the magnetic field to pass through them and into the specimen. The details of the experimental setup and heating process are important in achieving a homogeneous temperature field across the tin - parameters such as: distance between coil and specimen, power applied by the heater and quality of the cast tin sheet all influence the outcome of the experiment. Fig. 2b shows a sheet of silicone rubber laid across the upper ring; emery cloth is glued to the upper surface of the latter to provide high friction with the silicone diaphragm. Circular carbon-nylon / tin specimens measuring 130 mm in diameter are placed on top of the lower silicone diaphragm. Breather cloth and two connection ports were also placed onto the silicone sheet. In Fig. 2c a second silicone sheet was placed over the specimen and connection ports. A third Perspex ring, also with emery cloth bonded on its underside, was placed on top of the upper silicone sheet. Fig. 2c shows how an air-tight seal was created using thirteen G-clamps positioned around the Perspex rings and shows a vacuum connection and a pressure gauge attached to the upper silicone sheet facilitating pressure measurement during the experiments.

2.2.3. Upper thermoforming setup

A multi-step forming tool was manufactured and fitted into the test machine. Fig. 3a shows the steel tool suspended in the test machine. It consists of a long central solid cylinder surrounded by four progressively shorter annuli. At the top is a cap that attaches to the test machine. The internal geometry of the upper housing is shown in Fig. 3b. The activating force of the tool is its own weight (~63 kg in total). As the tool is lowered onto a flat surface, the central cylinder touches the surface first and transfers its weight onto the surface. As the tool continues to descend, the annuli also touch the surface, transferring their weight one after another, from the centre outwards. Once the bottom of all annuli (Fig. 3c) are flush with the flat surface, the upper end of the annuli are in contact with the internal 'roof' of the tool (Fig. 3b), from then on the tool acts as a solid rigid body. The test machine can now apply extra force down through the tool, onto the surface. The total diameter of the tooling is 130 mm. The central cylinder is 14 mm diameter and each annulus has a thickness of 14 mm. There is also a 1 mm gap between each annulus. The pressure applied by the weight of each segment is independent of area and is a function of material density and the height of the annulus. The pressure generated by the weight of the steel tool ranged from 47.2 kPa to 51.2 kPa with differences due to variation in the length of the segments required by the design of the upper tool housing

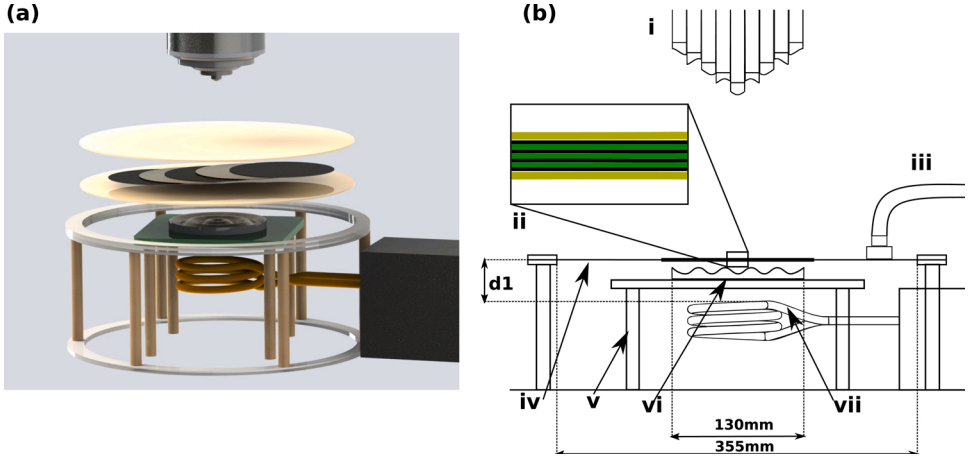

Fig. 1. (a) 3d construction of thermoforming set up with diaphragm and samples exploded (b) Sectioned schematic of the induction thermoforming setup. (i) multistep male tooling with segmented ripple tooling attached, (ii) exploded view of tin and nylon layup (yellow represents the silicone diaphragm sheets, black is carbon-nylon composite and green is tin interlayer), (iii) vacuum pump connector, (iv) blank holder, (v) epoxy-glass fibre false base plate, (vi) female ripple tooling and (vii) solenoid induction coil. d1 refers to the distance between coil and sample. d1 = 25 mm for forming of flat samples, and d1 = 60 mm when forming ripple specimens.

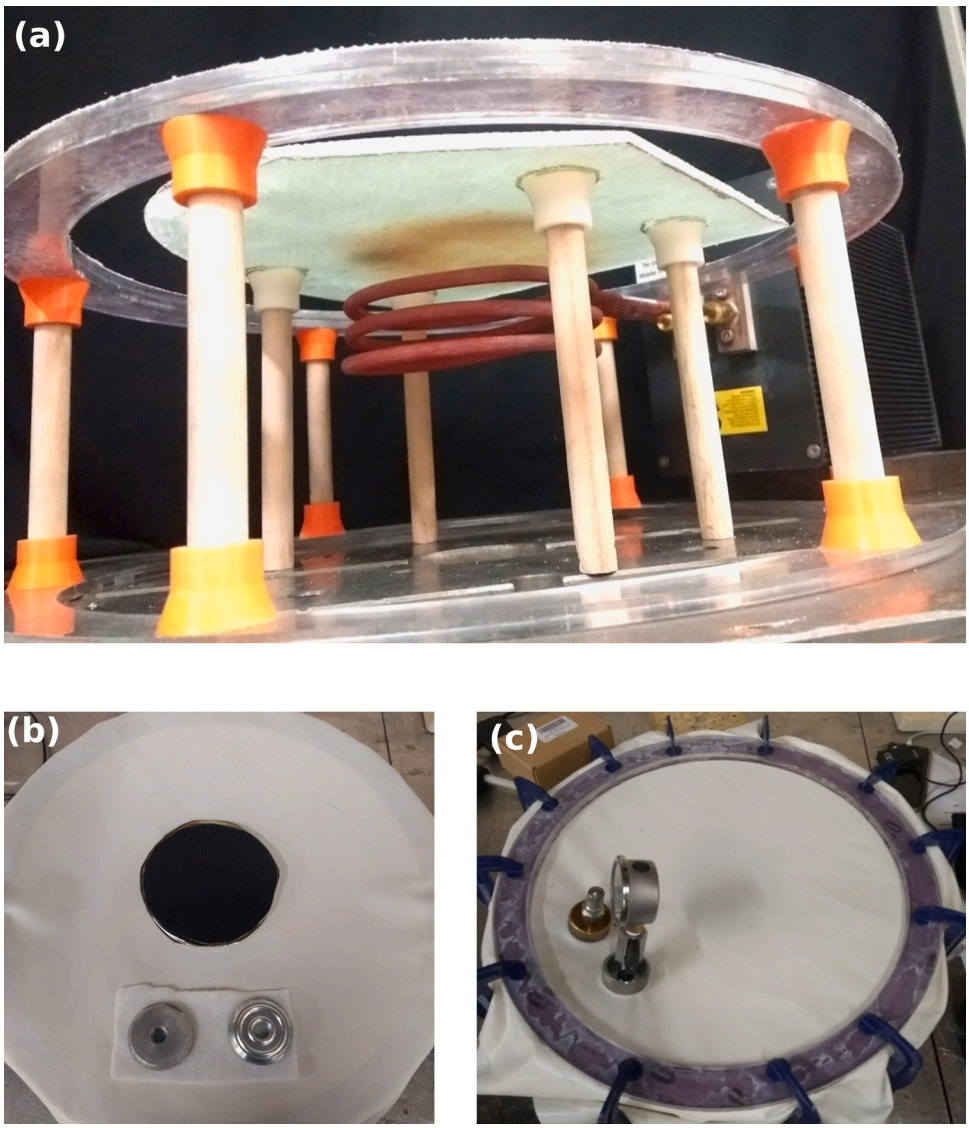

Fig. 2. (a) Helical induction heating coil positioned below a 'false base-plate' positioned above induction coil and below silicone diaphragm, (b) internal set up of silicone diaphragm containing sample and vacuum connectors and (c) diaphragm back secured in place with clamps.

(See Fig. 3).

2.2.4. Segmented matched die geometry

The chosen geometry has a topology resembling a ripple on a pond. Fig. 4 shows a cross section along the diameter of the segmented male and female tooling in both closed (Fig. 4a) and open (Fig. 4b) positions. The male tooling follows a cosine curve with an amplitude of 6 mm and a wavelength of 26 mm. There are five waves across a total diameter of 130 mm. The female tool is then offset with a constant gap of 1.74 mm to accommodate the material thickness. The shape was chosen as it is ideal for future parametric study; it can be made more or less challenging to form simply by changing the amplitude of the 'ripples' on the geometry. Fig. 5a shows a cross section of the segmented male tooling, while Fig. 5b shows a cross section of the single piece female tooling. Fig. 5c shows the segmented 3d printed ABS plastic male tooling while Fig. 5d shows the 3d printed ABS plastic female tooling. The use of 3d printing allowed for rapid manufacture of a non-conducting and non-magnetisable tooling that would not heat in response to the induction heater. The tooling was printed using a Stratasys F270 FDM machine with an accuracy of ± 0.2 mm.

3. Thermo-forming experiments

3.1. Induction heating

The primary metallic allotrope of tin, white β tin, is a paramagnetic material which can be heated via induction heating. An induction heater involves a high frequency alternating current passing through an electromagnet. This creates rapidly changing magnetic fields which then generate small eddy currents in the magnetic material to be heated. A key factor in optimising induction heating is the 'skin effect'. This is the tendency for the eddy currents to be concentrated near the surface of a body. The skin depth, δ, is defined as the depth in which 87 % of power is dissipated and can be calculated as,

$$\delta = \sqrt{\frac{2\rho}{\mu\omega}} \tag{1}$$

where ρ is the resistivity of the material, μ is the absolute magnetic permeability [41] and ω is the frequency (Hz). Note that, $\mu = 1.256 \times 10^{-6}$ Hm^{-1} and for tin, $\rho = 1.09 \times 10^{-7}$ Ωm. A skin depth of 0.5 mm occurs at a frequency of ~100 kHz. It can also be shown that ~98 % of

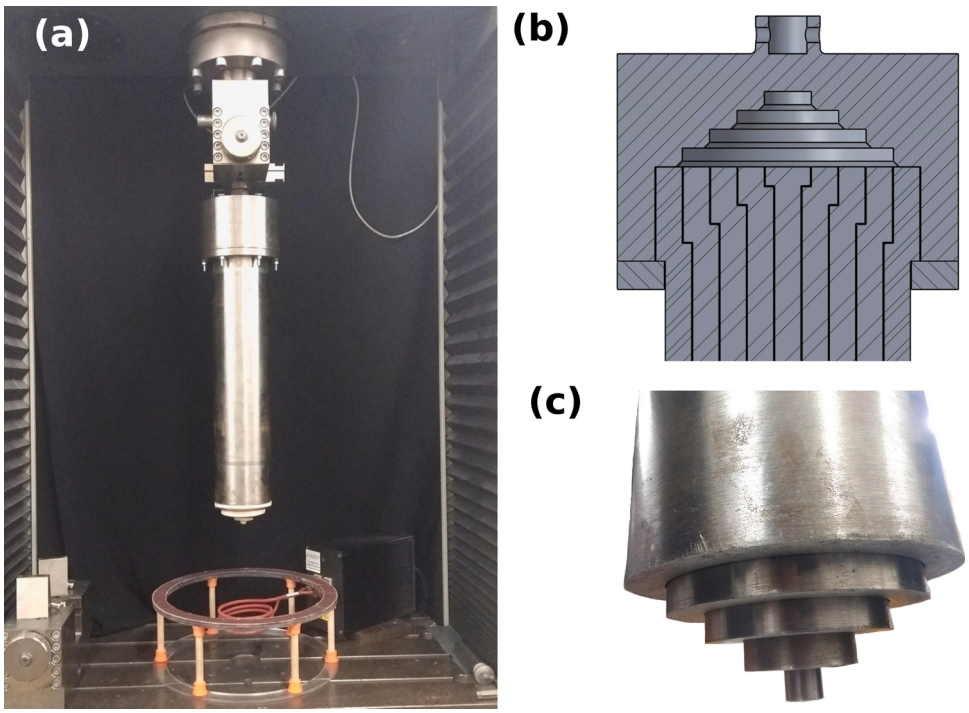

Fig. 3. (a) Reconfigurable multi-step tool fitted inside a universal test machine. End of tooling fitted with 3d printed ABS ripple tooling, (b) internal geometry of the upper housing of the multistep tooling in free hanging position and (c) close-up showing the end of the steel tool.

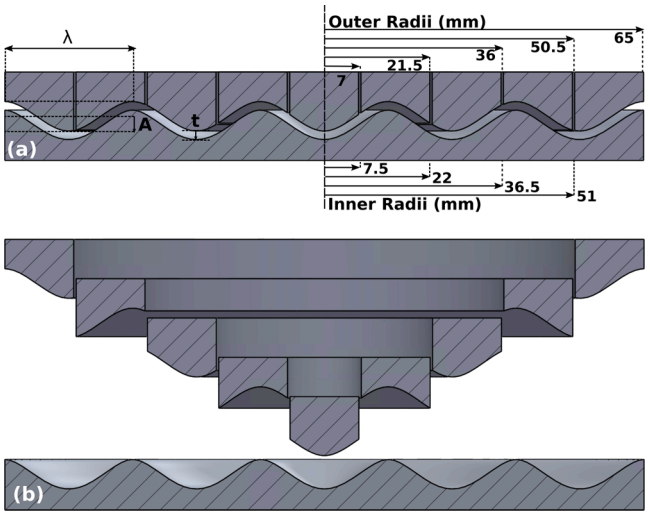

Fig. 4. (a) Cross section of male and female rippled tools in closed position. Wavelength, λ, is 26 mm, Amplitude, A, is 6 mm and tool gap, t, is 1.74 mm. The outer radii of the central cylinder and four annuli are marked along with the inner radii of the four annuli on the right side. (b) cross section of female tooling and segmented tips for male tooling in open position.

power is dissipated within two skin depths [39]. Thus, the thickness of the tin sheet was chosen as 1 mm. Despite the tin's molten state and being subject to 1 bar of normal pressure, due to the lack of pressure gradient inside the diaphragm there was no obvious flow of the tin out of the specimen prior to the forming process.

3.2. Experimental challenges

Creating a uniform temperature across the tin sheet is a non-trivial process and was one of the greatest causes of variability within the investigation. The heating of the specimen is a function of numerous parameters including, for example, the: (i) heater power, (ii) distance between induction coil and specimen, (iii) relative position of coil and specimen in (x, y) plane, (iv) specimen size and shape, (v) heat transfer between tin, composite and rubber diaphragm, (vi) temperature measurement system (vii) and flow of tin within the specimen. Achieving accurate and reliable temperature control is extremely challenging. The temperature of the specimen was measured on the upper surface of the silicone diaphragm with a thermal camera and laser thermometer as detailed in Section 2.2.2. Due to the small dimensions in the z-direction and the fact that silicone can be semi-transparent in the wavelengths used by the cameras it was assumed that temperature variation through the stack would be small. There was temperature variation in the (x, y) plane due to the lower thermal conductivity of the nylon and flow of the molten tin leading to non-uniform heat generation.

Temperature control was attempted by manually controlling the induction coil generator power (up to 6 kW) and by manually adjusting the position of the induction coil during the heating process, based on real-time feedback from the two temperature measurement techniques (thermal camera & laser thermometer). Fig. 6 shows images from the thermal camera, Fig. 6a shows the heating of a tin-carbon-nylon layup (with no rubber diaphragm) using a high power (10 kW) showing the localisation of hotspots. Fig. 6b and Fig. 6c show heating of a tin and carbon-nylon layup when placed within the diaphragm sheets and using lower power (6 kW). The image demonstrates improved temperature homogeneity. The aim was to produce an evenly distributed temperature profile across the specimen, hot enough to melt the tin and composite matrix phase while avoiding localised hot spots that could lead to failure of the diaphragm. A surface temperature reading of 250 °C was the criteria used to initiate forming tests. This took approximately five minutes when heating two-layer specimens, and approximately ten minutes when heating four-layer specimens. Inevitably manual control led to variable results, with failure rates decreasing to around 30 % as the experimenter became more practiced. An improved setup with more refined feedback-based heating control, informed by greater understanding gained through process modelling, would likely reduce failure rates.

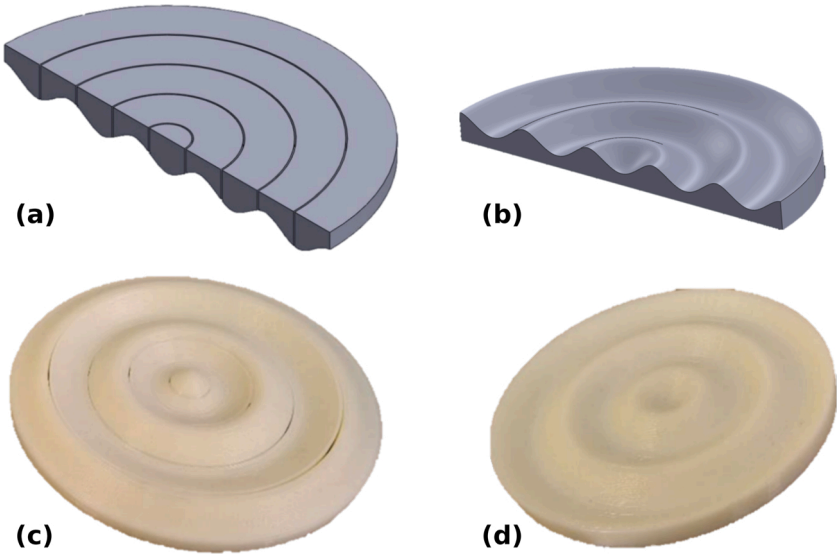

Fig. 5. (a) CAD showing cross section through segmented male ripple tool (b) cross section through female ripple tool, (c) 3-d printed ABS segmented male ripple tool, (d) 3-d printed ABS single piece male ripple tool.

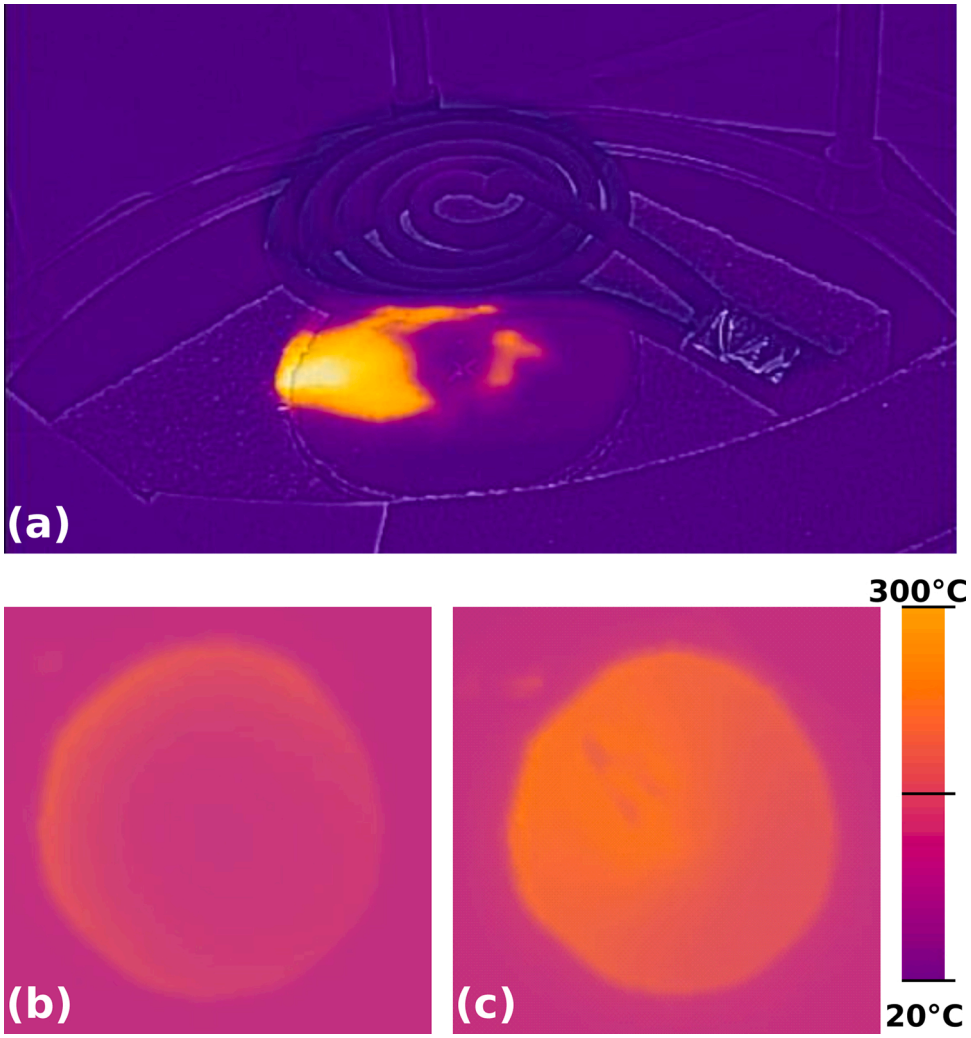

Fig. 6. Captured Images from IR camera. (a) 10 kW heating of nylon-carbon tin layup with hotspots (no rubber diaphragm sheet). (b) 6 kW heating of tin and carbon-nylon layup within silicone diaphragm after 30 s. (c) 6 kW heating of tin and carbon-nylon layup within silicone diaphragm after 300 s. Scale bar refers to (b) and (c).

Another major challenge in the experiments was related to the polymeric nature of the male and female ripple tooling used in the investigation. Because the tooling had to be non-conducting the only option available within the timeframe of the project was 3-d printed ABS tooling. ABS has a glass transition temperature of ~110 °C and is usually printed at ~230 °C. Consequently, it becomes soft well below temperatures required to melt tin and nylon. As a result, and despite being thermally protected to some degree by the rubber diaphragm, the ABS tooling was inevitably exposed to high temperatures and therefore prone to distortion during forming. Consequently, it had to be re-printed several times throughout the investigation due to loss of shape. Despite these challenges, a large test matrix was conducted (20 experiments in total) and meaningful results were obtained. In the following section, a selection of results from the full investigation are presented and discussed.

3.3. Multi-step press forming

Selected results from the induction melt-forming process are presented. The experiments begin with expulsion of a single sheet of tin from a flat specimen and gradually increase in complexity towards the forming of a multi-axial layup using the ripple tool described in Section 2.2.4. Tests demonstrate that at least three sheets of tin can be simultaneously melted using an appropriate induction heating system.

3.3.1. Consolidation of a flat plate with one layer of tin

Initial tests looked at two preconsolidated carbon-nylon sheets and a single layer of tin. All sheets were circular with a 130 mm diameter. A layup of $[0°/90°/90°/0°/\overline{T}]_S$ was tested. "T" is used to represent a layer of interlaminar tin of 1 mm thickness. Initial testing used a plastic prototype of the multi-step forming tool (pressure due to self-weight = 10 kPa) with the specimen layup held under vacuum inside the silicone rubber diaphragm. The specimen was heated until a diaphragm surface temperature of 250 °C was achieved, then pressed at 500 mm/min against the flat false base-plate to analyse the expulsion of the tin. Only the pressure due to the vacuum and self-weight of the tooling itself was used and no extra consolidation pressure was applied. The result is shown in Fig. 7a (plan view) and in Fig. 7b (internal cross-section). Fig. 7a shows that the tin flowed out of the side of the specimen due to the squeeze flow. Visual inspection of the cross-section (Fig. 7b) suggests a low residual tin content.

3.3.2. Consolidation of a flat plate with three layers of tin

This test used the multi-step forming tool with four circular nylon sheets stacked together with 3 tin interlayers. The layup used was $[0°/90°/90°/0°/T/90°/0°/0°/90°/\overline{T}]_S$. All sheets were 130 mm in diameter. The specimen was held under vacuum inside the silicone rubber diaphragm. The specimen was heated until a diaphragm surface temperature of 250 °C was achieved, then pressed at 500 mm/min against the flat false base plate to analyse the expulsion of the tin. Only the pressure due to vacuum and the self-weight of the tooling itself (50 kPa) was used and no extra consolidation pressure was applied.

A selected result is shown in Fig. 8a (plan view) and in Fig. 8b (internal cross section). Initial visual inspection of the cross section (Fig. 8b) indicates a low residual tin content. A total of six tests were performed. In one of these, full melting of the interlaminar tin was not obtained (i.e. a small region of undeformed tin sheet with no bonding between nylon plies was left behind), deeming that test a failure. The other five were successful in both obtaining full melting and in removing a significant proportion of the interlaminar tin (see Section 3.4.1).

3.3.3. Ripple forming using a single layer of tin I

This test used the steel multi-step tool to form a specimen containing one tin layer with a layup of $[0°/90°/90°/0°/\overline{T}]_S$. The layup is held under vacuum inside the silicone rubber diaphragm. The 3-d printed female tool (see Fig. 5d) was placed on the false base-plate. The ABS segmented male tool (see Fig. 5c) was temporarily attached to the steel multi-step forming tool using weak adhesive. The specimen was heated until molten, then pressed at 500 mm/min between the male and female ripple tools. The result is shown in Fig. 9a (plan view) and in Fig. 9b (internal cross-section). The cross section reveals good expulsion in some regions, but poor in others with significant amounts of residual tin. The surface quality of the formed ripple shape is good, the multi-step forming process appears to successfully mitigate damage to the surface of the composite part due to drag across the tooling. A total of five samples were carried out with this layup with 4 being deemed successes and 1 being deemed a failure.

3.3.4. Ripple forming using a single layer of tin II

A similar test set-up to that used in Section 3.3.3 was employed, though here the orientation of the carbon layers was changed to $[0°/90°/90°/0°/T/-45°/45°/45°/-45°]$. This layup introduces much greater translational displacement between neighbouring plies offering the opportunity to investigate the ability of the tin layer to reduce inter-ply friction and to mitigate wrinkling. The result is shown in Fig.10a (plan

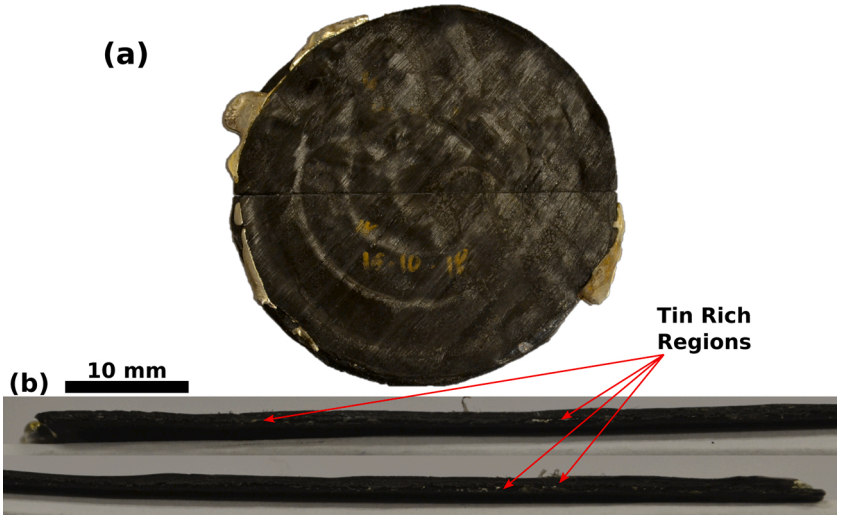

Fig. 7. Single layer of tin expelled from two carbon-nylon laminates $[0°/90°/90°/0°/\overline{T}]_S$. (a) plan view showing cutting line, (b) cross-section along cutting line showing small traces of residual tin (above, from left edge to centre, below from centre to right edge).

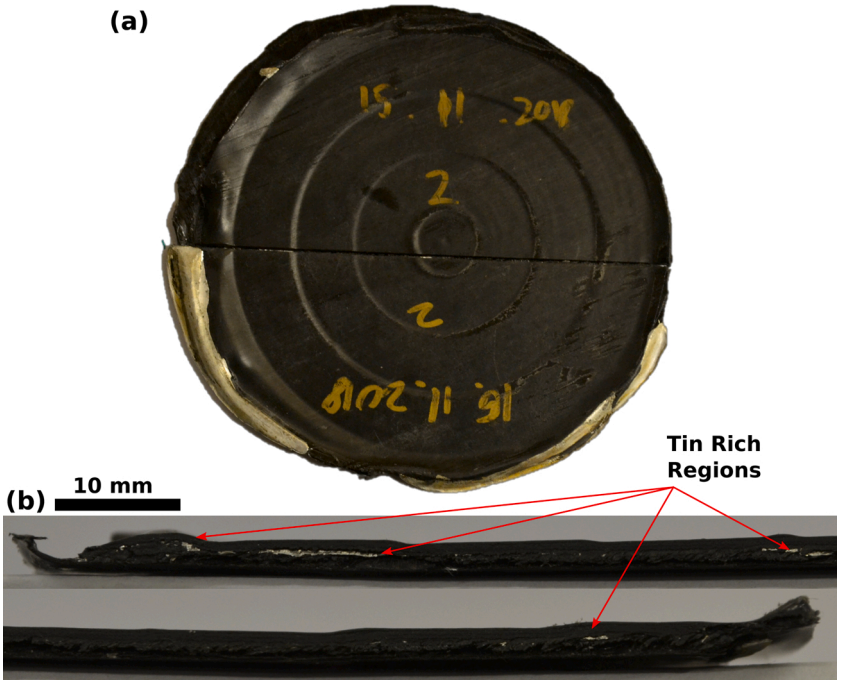

Fig. 8. Three layers of tin expelled from four carbon-nylon laminates $[0°/90°/90°/0°/\ T/90°/0°/0°/90°/\ \overline{T}]_S$ (a) plan view showing cutting line, (b) cross-section along cutting line showing small traces of residual tin (above, from left edge to centre, below from centre to right edge).

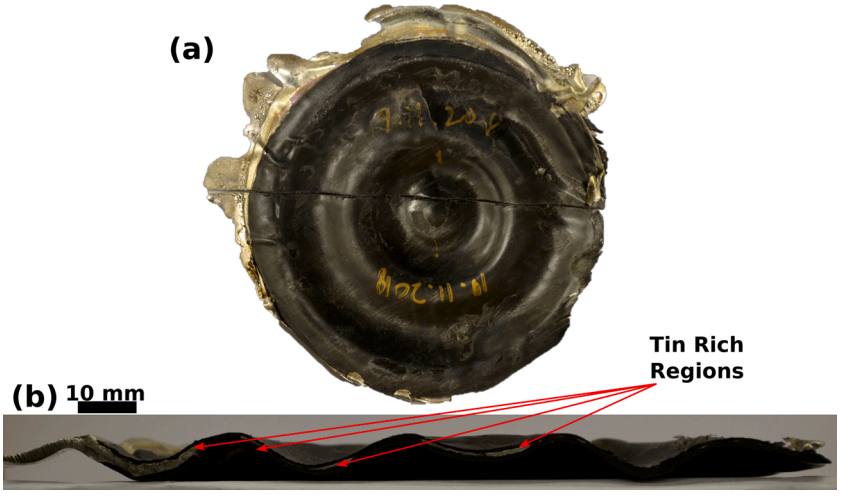

Fig. 9. One layer of tin expelled from two carbon-nylon laminates $[0°/90°/90°/0°/\ \overline{T}]_s$. (a) plan view prior to cutting and (b) cross-section along cutting line showing very little residual tin along the right-hand section but significant amounts of residual tin in the left-hand section.

view), Fig. 10b (oblique view), and Fig. 10c (internal cross-section). Fig. 10a reveals wrinkles across the upper right-hand side of the formed specimen, but a smooth, defect free appearance across the lower-left portion of the specimen. The wrinkles are shown more clearly in Fig. 10b It was noted in both this and in several other experiments (not reported here) that the defect free side of the specimen was usually correlated with the side showing the greatest flow of exiting liquid tin. It thus seems plausible that the tin is acting as a lubricant, however there are other potential explanations such as regions of higher laminate temperature correlating with high tin content. The cross-section shown in Fig. 10c reveals good tin expulsion in some regions but poor in others.

3.3.5. *Ripple forming using two layers of tin*

Finally, specimens consisting of two tin interlayers and three pre-consolidated cross-ply carbon/nylon laminates were tested with a layup of $[0°/90°/90°/0°/T/-45°/45°]_s$. The layup introduces two interfaces that undergo high translational displacements. The result is shown in Fig. 11a (plan view) and Fig. 11b (internal cross section). Fig. 11a shows that there are no obvious wrinkles from above and there is a high level of symmetry. Due to softening of the female polymeric tooling (see Section 3.2), the laminate has not conformed to the ripple shape of the tooling and has flattened on the left side. Nevertheless, the internal cross section in Fig. 11b shows good removal of the tin interlayer across most of the cross section but with significant localised residual tin on the righthand side. Four similar tests were performed however three were deemed failures due to the laminates not conforming to the desired ripple shape due to a softening of the female polymer tooling.

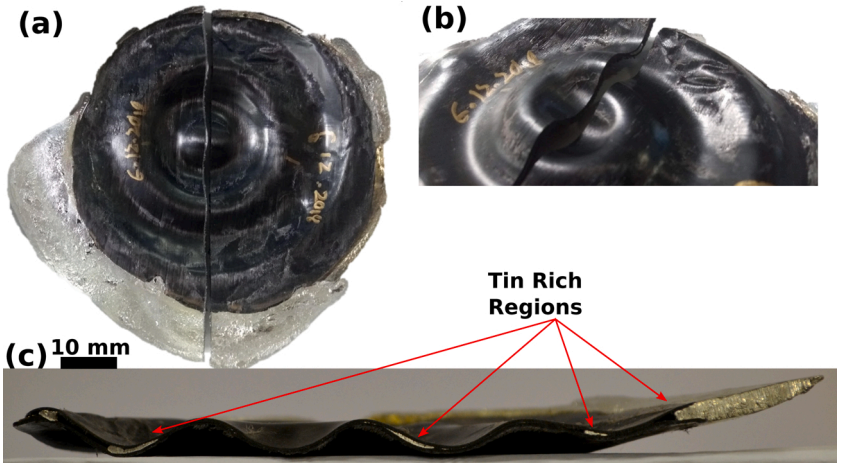

Fig. 10. Second attempt with one layer of tin expelled from two carbon-nylon laminates [0°/90°/90°/0°/T/-45°/45°/45°/-45°]. (a) plan view and (b) cross-section along cutting line showing very little residual tin along most of the cross-section. Tin does however, tend to 'stick' at corners.

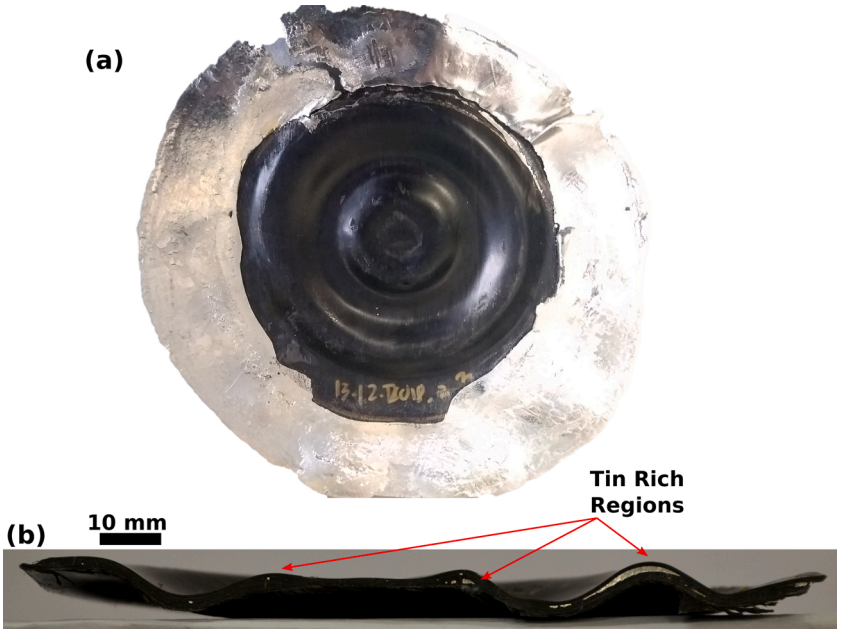

Fig. 11. Attempt with two layers of tin expelled from three carbon-nylon $[0°/90°/90°/0°/T/-45°/45°]_s$. (a) plan view and (b) cross-section along cutting line showing little residual tin along most of the cross-section.

3.4. Residual tin content

In this Section, a brief report of residual tin contents, measured using X-ray and micro CT, is provided.

3.4.1. Residual tin - flat plates

Table 1 shows the volume of residual tin (as a percentage of final part volume) for a selection of the flat consolidated discs. The scans were carried out using a Nikon XT H 225/320 LC Computer Tomography system. The samples were scanned at 140 kV and 136 μA and the processing was handled in Simpleware ScanIP. Results show tin volumes consistently below 5–10 % when heating and forming multilayer flat specimens, demonstrating the basic principle of the multistep tooling, i.e. generation of a squeeze flow capable of expelling most of the interlaminar tin. Further radiographic work is planned for a future paper.

3.4.2. Residual tin - ripple geometry

Table 2 shows the volume of residual tin as a percentage of the volume for the formed ripple geometry parts. These samples were scanned with a 170 kV X-ray generator with an exposure of four seconds. The output was then digitised and processed in MATLAB. The tin volume percentages in Table 2 are considerably higher than for the flat discs, ranging from 8 to 32 %. In addition to the challenges discussed in Section 3.2, several factors increased the comparative difficulty in expelling

Table 1
Residual tin volume as a percentage of final part volume for $[0°/90°/90°/0°/T/90°/0°/0°/90°/\overline{T}]_S$ layup on flat plate, determined using CT scans. Uncertainties relate to the resolution of the CT scan (~50 μm).

Test	Residual Tin Volume (%)	Volume of Original Tin Interlayer Removed (%)
1	$5.7 \pm^{4.1}_{2.6}$	$97.0 \pm^{2.1}_{1.4}$
2	$4.2 \pm^{2.4}_{1.6}$	$97.8 \pm^{1.3}_{0.9}$
3	$1.5 \pm^{0.8}_{0.5}$	$99.4 \pm^{0.2}_{0.4}$
4	$2.5 \pm^{2.2}_{1.3}$	$98.6 \pm^{0.8}_{1.3}$
5	$1.6 \pm^{1.6}_{0.9}$	$99.0 \pm^{0.5}_{0.9}$

Table 2
Residual tin volume as percentage of final part volume for ripple geometries. Determined from X ray scans of part. Uncertainties relate to the resolution of the X-ray (~0.2 mm).

Test number	*Layup*	*Residual Tin Volume (%)*	Volume of Original Interlayer Removed (%)
6	$[0°/90°/90°/0°/\overline{T}]_s$	$18.2\pm^{5.6}_{6.2}$	$82.4\ \pm^{6.0}_{5.4}$
7	$[0°/90°/90°/0°/\overline{T}]_s$	$11.4\pm^{3.7}_{4.5}$	$88.8\pm^{4.4}_{3.6}$
8	$[0°/90°/90°/0°/\overline{T}]_s$	$15.9\pm^{5.0}_{5.6}$	$86.4\pm^{4.8}_{4.3}$
9	$[0°/90°/90°/0°/\overline{T}]_s$	$15.2\pm^{5.0}_{4.5}$	$83.9\pm^{4.8}_{5.2}$
10	[0°/90°/90°/0°/T/-45°/45°/45°/-45°]	$20.2\pm^{7.5}_{6.4}$	$81.2\pm^{6.9}_{6.0}$
11	[0°/90°/90°/0°/T/-45°/45°/45°/-45°]	$12.3\pm^{4.1}_{5.0}$	$86.8\pm^{5.4}_{4.4}$
12	[0°/90°/90°/0°/T/-45°/45°/45°/-45°]	$32.4\pm^{9.7}_{10.6}$	$72.4\pm^{8.8}_{8.0}$
13	[0°/90°/90°/0°/T/-45°/45°/45°/-45°]	$11.1\pm^{3.5}_{4.2}$	$88.4\pm^{3.7}_{4.4}$
14	$[0°/90°/90°/0°/T/-45°/45°]_s$	$8.3\pm^{3.2}_{4.2}$	$96.4\pm^{1.9}_{1.4}$

tin for the ripple geometry. The first was tooling misalignment and tooling tolerances; deviations in tool axis alignment, or inaccuracies in the rather coarse 3-d printed male and female tool surface geometries could alter the pressure gradient acting on the molten tin. The segmented male tooling was also manufactured with large tolerances, resulting in small gaps between annuli (up to 1 mm, see Fig. 4) potentially resulting in low pressure areas that could disrupt the outward pressure gradient. The complex shape of the ripple geometry also caused significant shear deformation of the nylon carbon fibre laminate leading to varying laminate thickness. Given the designed gap between the tools is constant at 1.74 mm thickness, this would lead to regions of relatively high and low pressure, again disrupting the squeeze flow out of the laminate.

High levels of residual tin are potentially detrimental for two main reasons. First, they will increase the mass of the final part. Tin is much denser than a carbon fibre reinforced nylon sheet (~7300 kg/m^3 vs ~1500 kg/m^3) and, as such, even 3 % of the volume as tin would increase the mass of a part by ~12 %, and 10 % would increase the mass by ~40 %. Secondly, the presence of tin replaces interlaminar nylon bonds with a nylon-tin-nylon interface. Strong hydrogen bonds form between nylon molecular chains and these are unlikely to form with a tin lattice resulting in a weaker interface. This may result in reduced interlaminar shear strength, though the mechanical characterisation of the formed samples will be published in a future paper.

4. Conclusions and future work

This work explores the feasibility of heating, forming and consolidating multi-axial carbon-nylon composite laminates into complex multi-cavity geometries. A novel reconfigurable multi-step forming tool has been designed and manufactured and shown to provide a mechanism to generate the required pressure driven squeeze flow to expel molten tin from the laminate during forming. Use of induction heating coupled with tin interlayers has been demonstrated to be a fast and effective method of heating the laminate from within. There is some evidence to suggest that wrinkling defects are mitigated when forming complex geometries containing multiple cavities, due to the lubricating effect of molten tin, though further work is required to establish this possibility more firmly. The multi-step forming tool can be fitted into a press or universal test machine for both induction-melt forming or thermo-forming after radiant heating. Consequently, future work will focus on a direct comparison of the quality of parts formed following the two different heating methods. At present, the process is far from perfect with failure rates at the end of the investigation running at around 30 %. It has been possible to reach residual tin volumes of less than 5 % when consolidating a flat plate, however when forming ripple geometries, 8–32 % of the final part volume was residual tin. The influence of such high tin contents is likely to be severely detrimental to the specific mechanical properties of the laminate and future work is planned to characterise the mechanical behaviour as a function of tin content. However, the design implemented here is a first attempt and significant refinements can easily be made to reduce residual tin content (e.g. using ceramic rather than polymer tooling, improving machining tolerances, improving the induction heating control and improving understanding of the underlying physics involved in the process). This short investigation leaves many unanswered questions regarding both the quality of the formed parts and the reliability of the process. Further improvements in the process were not possible due to the time constraints imposed by equipment rental. Nevertheless, the basic concepts have been shown to be feasible, albeit requiring significant improvements if they are to combine to create a viable processing route. Given the potential advantages of faster, more energy efficient processing and reduced wrinkling, we believe the process merits further investigation. Indeed, if properly controlled, melt induction forming could offer a step-change in performance compared to existing advanced composite press-forming technology. The main obstacle in attaining these advantages lies in improving control and fundamental understanding of the process.

Declaration of Competing Interest

The authors report no declarations of interest.

Acknowledgements

The authors would like to acknowledge the support of the Engineering and Physical Sciences Research Council (EPSRC) via a feasibility study funded by EP/P006701/1 and a DTA PhD studentship (for Iain Campbell) funded by EP/N509668/1.

References

[1] Haanappel SP, Ten Thije RHW, Sachs U, Rietman B, Akkerman R. Formability analyses of uni-directional and textile reinforced thermoplastics. Compos Part A Appl Sci Manuf 2014;56:80–92. https://doi.org/10.1016/j.compositesa.2013.09.009.

[2] Harrison P, Gomes R, Curado-correia N. Composites: part A Press forming a 0 / 90 cross-ply advanced thermoplastic composite using the double-dome benchmark geometry. Compos Part A 2013;54:56–69. https://doi.org/10.1016/j.compositesa.2013.06.014.

[3] Liu K, Zhang B, Xu X, Ye J. Experimental characterization and analysis of fiber orientations in hemispherical thermostamping for unidirectional thermoplastic composites. Int J Mater Res 2019;12. https://doi.org/10.1007/s12289-018-1410-y.

[4] Guzman-Maldonado E, Hamila N, Naouar N, Moulin G, Boisse P. Simulation of thermoplastic prepreg thermoforming based on a visco-hyperelastic model and a thermal homogenization. Mater Des 2016;93:431–42. https://doi.org/10.1016/j.matdes.2015.12.166.

[5] Lessard H, Lebrun G, Benkaddour A, Pham X-T. Influence of process parameters on the thermostamping of a [0/90]12 carbon/polyether ether ketone laminate. Compos Part A Appl Sci Manuf 2015;70:59–68. https://doi.org/10.1016/J.COMPOSITESA.2014.12.009.

[6] Wang P, Hamila N, Boisse P. Thermoforming simulation of multilayer composites with continuous fibres and thermoplastic matrix. Compos Part B Eng 2013;52:127–36. https://doi.org/10.1016/J.COMPOSITESB.2013.03.045.

[7] McCool R, Murphy A, Wilson R, Jiang Z, Price M, Butterfield J, et al. Thermoforming carbon fibre-reinforced thermoplastic composites. Proc Inst Mech Eng Part L J Mater Des Appl 2012;226:91–102. https://doi.org/10.1177/1464420712437318.

[8] O'Brádaigh CM, Pipes RB, Mallon PJ. Issues in diaphragm forming of continuous fiber reinforced thermoplastic composites. Polym Compos 1991;12:246–56. https://doi.org/10.1002/pc.750120406.

[9] McGuinness GB, ÓBrádaigh CM. Effect of preform shape on buckling of quasi-isotropic thermoplastic composite laminates during sheet forming. Compos Manuf 1995;6:269–80. https://doi.org/10.1016/0956-7143(95)95020-Y.

[10] Ahn H, Kuuttila NE, Pourboghrat F. Mechanical analysis of thermo-hydroforming of a fiber-reinforced thermoplastic composite helmet using preferred fiber orientation model. J Compos Mater 2018;52:3183–98. https://doi.org/10.1177/0021998318762547.

[11] Ahn H, Kuuttila NE, Pourboghrat F. Effects of pressure, boundary conditions, and cutting reliefs on thermo-hydroforming of fiber-reinforced thermoplastic

composite helmet based on numerical optimization. J Thermoplast Compos Mater 2019. https://doi.org/10.1177/0892705719842631.
[12] Dörr D, Henning F, Kärger L. Nonlinear hyperviscoelastic modelling of intra-ply deformation behaviour in finite element forming simulation of continuously fibre-reinforced thermoplastics. Compos Part A Appl Sci Manuf 2018;109:585–96. https://doi.org/10.1016/J.COMPOSITESA.2018.03.037.
[13] Hou M. Stamp forming of fabric-reinforced thermoplastic composites. Polym Compos 1996;17:596–603. https://doi.org/10.1002/pc.10649.
[14] MacHado M, Murenu L, Fischlschweiger M, Major Z. Analysis of the thermomechanical shear behaviour of woven-reinforced thermoplastic-matrix composites during forming. Compos Part A Appl Sci Manuf 2016;86:39–48. https://doi.org/10.1016/j.compositesa.2016.03.032.
[15] Yin H, Peng X, Du T, Chen J. Forming of thermoplastic plain woven carbon composites: an experimental investigation. J Thermoplast Compos Mater 2015;28:730–42. https://doi.org/10.1177/0892705713503668.
[16] European Commission. Setting CO2 emission performance standards for new passenger cars and for new light commercial vehicles, and repealing Regulations. 2019.
[17] Okine RK. Analysis of forming parts from advanced thermoplastic composite sheet materials. J Thermoplast Compos Mater 1989;2:50–76. https://doi.org/10.1177/089270578900200104.
[18] Lin H, Long AC, Clifford M, Wang J, Harrison P. Predictive FE modelling of prepreg forming to determine optimum processing conditions. AIP Conf Proc 2007;907:1092–7. https://doi.org/10.1063/1.2729660.
[19] Strong AB, Hauwiller PB. Incremental forming of large thermoplastic composites. J Thermoplast Compos Mater 1989;2:122–32. https://doi.org/10.1177/089270578900200204.
[20] Chen S, McGregor OPL, Endruweit A, Elsmore MT, De Focatiis DSA, Harper LT, et al. Double diaphragm forming simulation for complex composite structures. Compos Part A Appl Sci Manuf 2017;95:346–58. https://doi.org/10.1016/j.compositesa.2017.01.017.
[21] Hallander P, Sjölander J, Åkermo M. Forming induced wrinkling of composite laminates with mixed ply material properties; an experimental study. Compos Part A Appl Sci Manuf 2015;78:234–45. https://doi.org/10.1016/j.compositesa.2015.08.025.
[22] Hallander P, Sjölander J, Petersson M, Andersson T, Åkermo M. Fast forming of multistacked UD prepreg using a high-pressure process. Polym Compos 2019. https://doi.org/10.1002/pc.25217.
[23] Krebs J, Bhattacharyya D, Friedrich K. Production and evaluation of secondary composite aircraft components—A comprehensive case study. Compos Part A Appl Sci Manuf 1997;28:481–9. https://doi.org/10.1016/S1359-835X(96)00148-0.
[24] Benkaddour A, Lebrun G, Laberge-Lebel L. Thermostamping of [0/90]n carbon/peek laminates: influence of support configuration and demolding temperature on part consolidation. Polym Compos 2018;39:3341–52. https://doi.org/10.1002/pc.24354.
[25] Gutowski TG, Dillon G, Chey S, Li H. Laminate wrinkling scaling laws for ideal composites. Compos Manuf 1995;6:123–34. https://doi.org/10.1016/0956-7143(95)95003-H.
[26] Sjolander J, Hallander P, Akermo M. Forming induced wrinkling of composite laminates: a numerical study on wrinkling mechanisms. Compos Part A Appl Sci Manuf 2016;81:41–51. https://doi.org/10.1016/j.compositesa.2015.10.012.
[27] Vanclooster K. Forming of multilayered fabric reinforced thermoplastic composites. 2009.
[28] Thompson AJ, Belnoue JPH, Hallett SR. Modelling defect formation in textiles during the double diaphragm forming process. Compos Part B Eng 2020;202:108357. https://doi.org/10.1016/j.compositesb.2020.108357.
[29] Bloom LD, Wang J, Potter KD. Damage progression and defect sensitivity: an experimental study of representative wrinkles in tension. Compos Part B Eng 2013;45:449–58. https://doi.org/10.1016/J.COMPOSITESB.2012.05.021.
[30] Potter K, Khan B, Wisnom M, Bell T, Stevens J. Variability, fibre waviness and misalignment in the determination of the properties of composite materials and structures. Compos Part A Appl Sci Manuf 2008. https://doi.org/10.1016/j.compositesa.2008.04.016.
[31] Vanclooster K. Forming of multilayered fabric reinforced thermoplastic composites. University of Leuven; 2009.
[32] Nosrat Nezami F, Gereke T, Cherif C. Analyses of interaction mechanisms during forming of multilayer carbon woven fabrics for composite applications. Compos Part A Appl Sci Manuf 2016;84:406–16. https://doi.org/10.1016/j.compositesa.2016.02.023.
[33] Nosrat Nezami F, Gereke T, Cherif C. Active forming manipulation of composite reinforcements for the suppression of forming defects. Compos Part A Appl Sci Manuf 2017;99:94–101. https://doi.org/10.1016/j.compositesa.2017.04.011.
[34] Hancock SG, Potter KD. Inverse drape modelling—An investigation of the set of shapes that can be formed from continuous aligned woven fibre reinforcements. Compos Part A Appl Sci Manuf 2005;36:947–53. https://doi.org/10.1016/j.compositesa.2004.12.001.
[35] Tam AS, Gutowski TG. Ply-slip during the forming of thermoplastic composite parts. J Compos Mater 1989;23:587–605. https://doi.org/10.1177/002199838902300604.
[36] Shuler SF, Advani SG. Transverse squeeze flow of concentrated aligned fibers in viscous fluids. J Nonnewton Fluid Mech 1996;65:47–74. https://doi.org/10.1016/0377-0257(96)01440-1.
[37] Culpin MF. The viscosity of liquid indium and liquid tin. Proc Phys Soc Sect B 1957;70:1069–78. https://doi.org/10.1088/0370-1301/70/11/307.
[38] Keene BJ. Review of data for the surface tension of pure metals. Int Mater Rev 1993;38:157–91.
[39] Harrison P, Alvarez MF, Correia N, Mimoso P. Characterising the forming mechanics of pre- consolidated nylon-carbon composite. 2018. p. 24–8.
[40] TenCate. Cetex® TC910 Nylon 6 n.d.
[41] Davies J. Conduction and induction heating. London: Peregrinus; 1990.